ESTIMATION OF CHLOROPHYLL-A CONCENTRATION FROM THE ATMOSPHERIC CORRECTION OF MISR DATA

SISIR KUMAR DASH', TASUKU TANAKA[3], HIROYUKI HACHIYA[3], AND YASUHIRO SUGIMORI[4]

Abstract

Multi Angle Imaging Spectro Radiometer (MISR) has a capability to observe the ocean surface from different viewing directions. Attempts were made to estimate the ocean surface reflectance and chlorophyll-a concentration using MISR data. The aerosol optical thickness (AOT), available from the MISR archive is compared with the results simulated using the 6S radiation transfer code. It turns out that the AOT values agree with each other up to 85% in certain areas in case-1 waters. Substituting the archive values of AOT into the radiative transfer process, we obtain the surface reflectance. This surface reflectance, in turn, is employed together with the in-water algorithm, to obtain the chlorophyll concentration maps for three viewing directions (aft, nadir and forward). The pattern of obtained chlorophyll map is reasonable. It is estimated thai an error of about 35% is involved in the radiance calibration and AOT. Hence, with best possibility, the surface reflectance is quantified and the chlorophyll maps were generated. When it is compared with the nadir observation, the forward viewing camera overestimates and the aft viewing camera underestimates the chlorophyll-a concentration especially in case-1 waters- In case-2 waters, the chlorophyll-a concentration shows similar patterns for the three different viewing directions. Due to lack of in-situ data, absolute chlorophyll values were ignored but errors were quantified for (he surface reflectance and the aerosol optical thickness with the 6S simulated results.

Keywords: MISR, 6S, AOT, Surface reflectance, Chlorophyll-a,

1. Introduction

In the atmospheric correction of ocean color data, the radiance backscattered from the water column (water-leaving radiance) has to be evaluated by correcting the radiance at the top of the atmosphere (TOA) for the scattering and the absorption in the atmosphere (Gordon and Morel, 1983). The amount of radiance that reaches at space borne ocean color sensors is relatively small due to the scattering in the atmosphere and absorption in the water column. The water leaving radiance is the optical property of the oceanic water which signifies the concentration of phytoplankton. its decay, carbon cycle, etc. In the atmosphere, the visible light is scattered by air molecules and aerosols; while in the ocean, it is absorbed and backscattered by planktons, water molecules, and etc. The propagation of light through atmosphere causes problem due to the strong forward scattering by aerosols and it varies with its size (Gordon and Wang, 1994) and the uncertainty of aerosol scattering is complicated while comparing with the air molecular scattering (Rayleigh scattering). During the

1. GiKtoic School of Science & Technology, Chiba University. 1-33. Yayoi-Cho, tnage-Ku, Chiba-shi, Japan.
I DcnHntcnt of Mechanical Hngiiiecring, Yamaguchi University. Japan.
i. Rewrch Center for Frontier Medical Engineering. Chiba University. I-33. Yayoi-Cho, Inage-Ku. Chiba-shi, iCReSOS. Udayana University. Kampus Bukit Jimbaran, Dcspwr, Bali. Indonesia

atmospheric correction procedure, considerations must be given to the aerosol optical thickness and its wavelength dependence. Besides, knowledge on the aerosol phase function and the single scattering albedo are required in the radiative transfer calculations (Gordon and Zhang, 1996, Kaufman et al., 1994, Nakajima et al., 1983, Wang and Gordon, 1993). The aerosol particles are characterized by their shape, size, chemical composition and total amount, which in turn determine their radiative characteristics. Remote sensing relies on the transmission of radiation by the Earth's atmosphere and therefore strongly affected by the aerosol radiative characteristics (Lenoble, 1993). In this context, the establishment of the climatology of aerosol characteristics for remote sensing has been one of major objectives of the scientific community in the last several decades (International Aerosol Climatology project (IACP), 1991). These characteristics must be given for each wavelength *(k),* and the essential parameters are the vertical profile of the scattering coefficient (as), absorption coefficient (aa) and the scattering phase function. Microscopically, all these parameters are dependent on shape, size and composition of aerosols and well approximated. So far, several conventional algorithms were proposed in the EOS era (Gordon, 1997; Das, et al., 2002; Haltrin, 2002) to estimate aerosol optical thickness (AOT) and water-leaving radiance with certain accuracies using the data from satellite sensors with one viewing direction. In these algorithms, the I sun glitter radiance and the whitecapsi radiance are assumed to be constant in all the spectral regions and estimated with the! sea surface roughness and wind speed respectively.

The present paper describes the direct I estimation of aerosol optical thickness and! surface reflectance using Multi-Angle I Imaging Spectro Radiometer (MISR) datan and the 6S code. In Section 3.1, we compare the AOT value provided using! MISR algorithm (David et al., 2001) with! that calculated using the 6S code. Based on the MISR AOT and other geometricall information from the MISR archive, wel estimate the surface reflectance asl described in Section 3.2. The surfacel reflectance, in turn, is employed to retrievel the chlorophyll-a concentration asl described in Section 3.3

II. Methodology

a. MISR Data

MISR is a sensor onboard the Terra satellite (launched in December 1999). It isl | equipped with three visible bands and one I near-infrared band, and views the earth in I nine different viewing directions to study I the scattered sunlight from different

Table: 1. Specification of MISR Instrument

Parameters	Value
Viewing angles (Degrees)	0.0 (nadir), 26.1,45.6, 60.0, and 70.5 in both fore and aft of nadir
Swath (Kilometers)	360
Spectral bands (nm)	446.4,577.5,671.7,866.4
Spectral bandwidth (nm)	41.9,28.6,21.9,39.7
Cross-track x along-track pixel sampling (commendable)	275 m x 275 m 550 mx 550 m 1.1 km x 1.1 km 275 km x 1.1 km

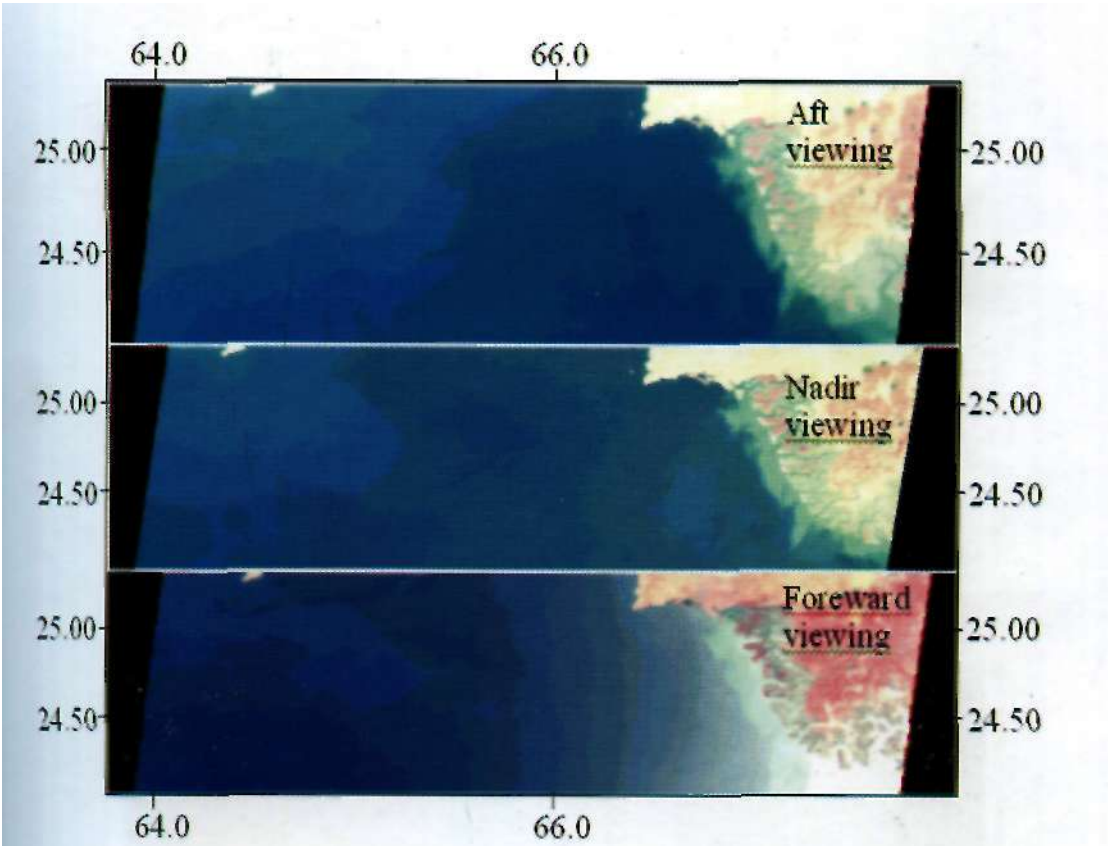

Figure 1. False color composite of MISR data on: 02 October 2003 (Path: 153, Block no: 71, MISR SOM P153 Block 71 Projection)

targets. Specifically, the MISR monitors the monthly, seasonal, and long-term trends in (1) the amounts and types of atmospheric particles (aerosols), including those formed by natural sources and by human activities, (2) the amounts, types, and heights of clouds, and (3) the distribution of land surface cover, including vegetation canopy structure. A detail configuration of the MISR instrument is described in Table-1.

The MISR data analyzed here were acquired on 2nd October 2003 over the Northwestern Arabian Sea (23°58'45.16"N to 25°21'42.85"N and 63°56'28.82E to 68°4'8.69"E). The MISR images for the three direction viewing camera A Forward (+26° inclination), Aft (-26°), and Nadir (0°) observations are denoted as AF, AA and AN, respectively. The false color composite (R: 446.4nm, G: 577.5, B: 671.7) is shown in Fig. 1, containing both in case-1 and case-2 waters. Land mask is not applied to the images to find out the minimum and maximum on the reflectance value at the TOA. The radiance *Li(k)* are converted to the apparent reflectance pr \k) at the TOA, using the expression

$$\rho_t(\lambda) = \frac{\pi L_t(\lambda)}{F_0(\lambda)\cos\theta_s} \quad \text{.....(1)}$$

here *Fo* is the extra-terrestrial solar irradiance, and 9_S is the solar zenith angle. The reflectances at the TOA for all four bands are shown in Fig. 2.

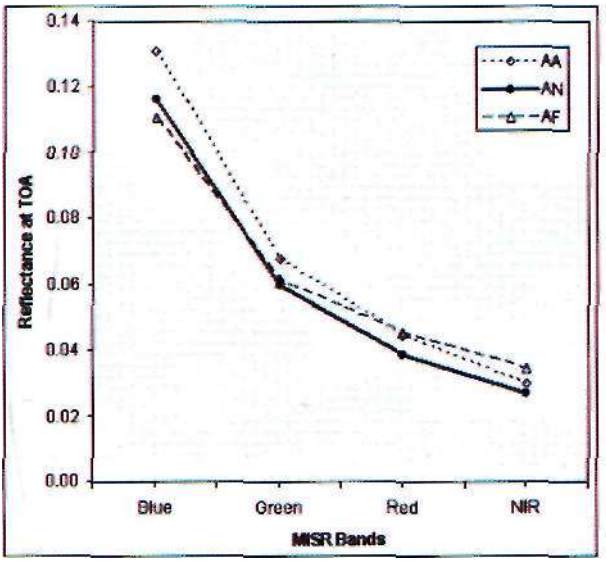

Figure 2. MISR reflectance at TOA

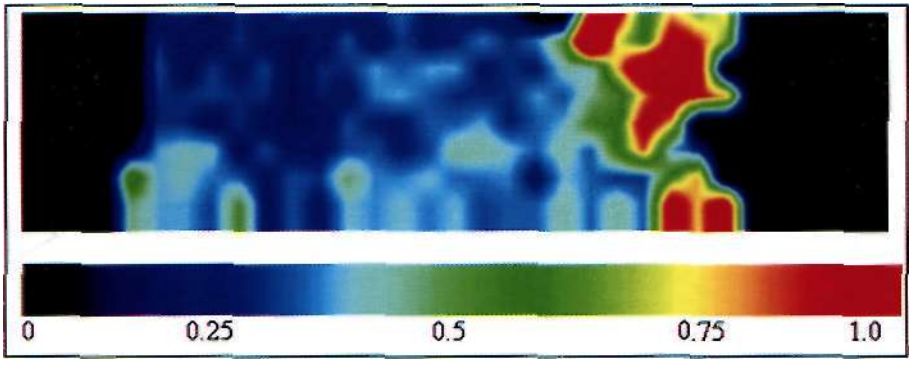

Figure 3: Aerosol optical thickness at 557.5nm derived from MISR archive

b. 6SCode

The 6S code is a widely used radiation transfer code which can accurately simulate the radiative transfer process in the atmosphere with limited computing resources and a fast approximation (Vermote, et al., 1997). The inputs to the 6S code in this research are zenith and azimuth angles for solar and satellite positions with the band wavelengths and satellite altitude parameters. In addition, the maritime aerosol model in the tropical regions is chosen for the present case. The 6S code calculates the radiance *L[k)* (or equivalently p/(A.) from Eq. (1)) for given values of surface reflectance *r(X)* and AOT (named as a variable Ta(X,)). Here, we need to evaluate *r(k)* and *Xa(k)* from the actually observed values ofL(A,). For this purpose, we employ the 6S code and we determine a set of *r\K)* and To (A.) which reproduces the value of p/(^) within an error range of + 0.00001 (reflectance unit).

III. Results and Discussion

Figure 2 shows the reflectance at the TOA obtained from the ocean part of the

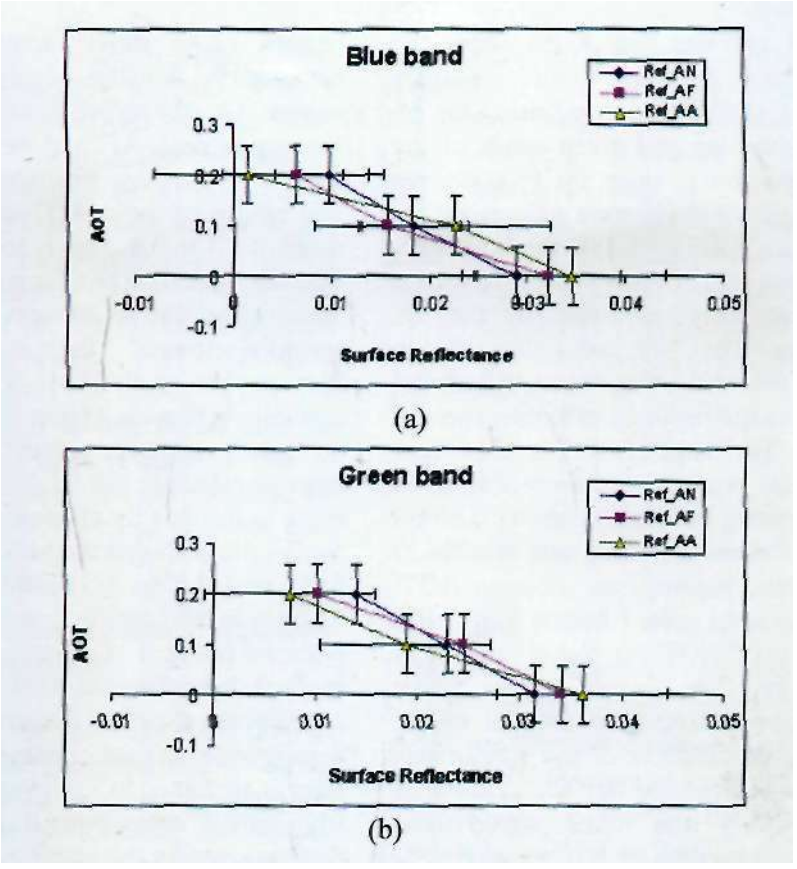

Fig. 4. Relationship between the aerosol optical thickness (AOT at 550 nm) and surface reflectance for blue and green bands

MISR data shown in Fig.l. In accordance with the post-calibration enor involved in the instrument, a 10% error is attached to the apparent reflectance (Bruegge, et al., 2004). In order to evaluate the corresponding enors in the AOT and surface reflectance, the mean value for each band is considered for pixels over the region under consideration. In the NIR band, the error range is significantly larger as compared to visible bands for all the AN, AA, AF cameras. For the error calculations, the data from each camera are separately treated. Here, the data from camera A is employed to estimate the AOT and the surface reflectance using the trial and error method. The MISR AOT is derived from the MISR archive and the AOT distribution for the study area is shown in Fig. 3.

a. Comparison of AOT values from the MISR archive and the 6S simulation

We have three observations for one pixel. Each observation is the function of two unknown variable $\tau_a(\lambda)$ andv. The detailed scheme to obtain the solution is as follows: (1) Let assume $\tau_a(\lambda) = 0$, then we can find three different $r(\lambda)$ for three different observations, which yield $\rho_t(\lambda)$ individually by the try and error application of the 6S code. (2) Then by changing$\tau_a(\lambda)$, we try to obtain a set of $\tau_a(\lambda)$ and $r(\lambda)$, where it satisfies $\rho_t(\lambda)$.

Fig. 4 (a) and Fig 4 (b) show the relationship between the surface reflectance and AOT derived using the 6S code for the blue and green bands of the MISR respectively. Since, the 6S code was used to estimate the ground reflectance for sensors like OCTS, MISR and MODIS etc., here we will not repeat the discussions on the accuracy involved in the 6S calculation. The best possible solution would be obtained using the multi viewing direction images without effecting spectral variations. The range of AOT is taken from Ramanathan et al, 2001, Rasch et al, 2000 before showing simulation results. The 6S code simulation is carried out directly in the visible regions to obtain AOT. However, as seen from Fig. 4(a) uncertainty of AOT for the blue band is quite large. The ocean region under investigation is free from the sun glitter. Under the assumption of the Lambertian surface, it is expected that the reflectance values from the three observation directions agree with each other within the error range. In some cases, the aft viewing camera (AA) shows some irregularity, occasionally it yields negative reflectance values. On the other hand, the forward viewing camera (AF) and the nadir viewing camera (AN) show positive AOT values. The ranges of these AOT values are in a range of 0.1 to 0.3. This is somewhat larger than the typical AOT of maritime aerosols, presumably, due to transportation of land aerosols toward the marine region (Ramanathan et al, 2001). The average of all these AOT with respect to the directions (except the negative values) are employed here, to calculate the 6S derived AOT and apply to the data for all viewing directions. Scatter plot between the MISR AOT (at 557.5 nm) and the AOT estimated with the 6S code (at 550 nm) in five selected pixels is shown in Fig. 5. Correction for the spectral dependence of AOT is considered small due to the small difference in these wavelengths. In case of marine aerosol, this error is attributed to a minimum percentage from the real estimation. It is quite evident that the error for the MISR AOT is larger than that from the 6S estimation in five

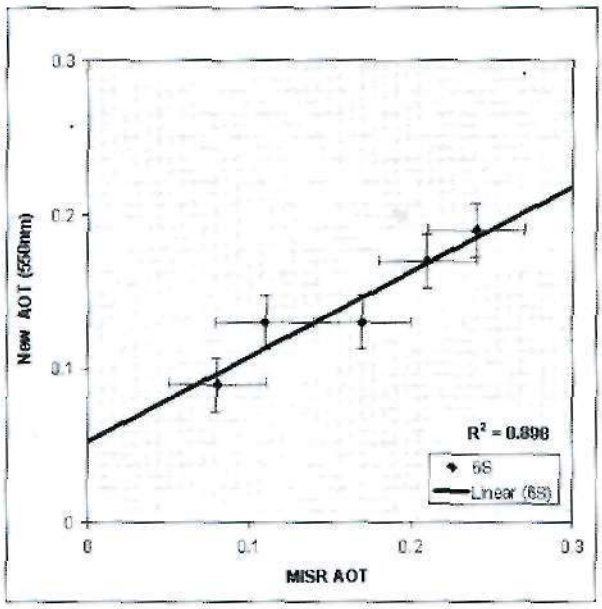

Figure 5 Scatter plot between MISR AOT (557.5 nm) and new AOT calculated using the 6S code (550 nm)

pixels shown in Fig. 5. Furthermore, this error estimation is a standard error estimation that pertained during data analysis and the radiative process incurred using 6S code. The range of both MISR and present AOT are quiet similar to the ranges from in situ measurements reported from the Indian Ocean Experiment (Ramanathan et al., 2001). The regression parameter (R2) between the MISR AOT and the new AOT is 0.898. Here the analysis is limited to few pixels and the distance between them is uniform. Due to the limited computational environment; all these pixels are 100% cloud free and dust free regions.

b. Estimation for surface reflectance and its uncertainty

The present estimation of AOT derived from the 6S code using the multi viewing images is limited to few geographical pixels. In order to estimate the surface reflectance, for a larger region, the most critical parameter is AOT *ia\k* Jtaken from the MISR archive, because the agreement of the MISR archive and the multi-viewing direction method are fairly good. Using Chandrasekhar's integration equation for the plane parallel atmosphere (Chandrasekhar, 1960) for the single scattering approximation, the radiative transfer equation can be shown as Eq. 2.

$$\rho_{total}(\tau, i_1, i_s) = \frac{\tau_r P_r(\cos\Theta) + \tau_a P_a(\cos\Theta)}{4\mu_1\mu_2} + r - \left(\frac{\tau_r}{2\mu_1} + \frac{\tau_r}{2\mu_s}\right) r - \left(\frac{\tau_r}{2\mu_1} + \frac{\tau_r}{2\mu_s}\right)(2-k)r \quad \ldots\ldots(2)$$

where, $\rho_{total}(\tau, i_1, i_s)$ is the reflectance at TOA., τ_r and τ_a are the optical thickness for Rayleigh and aerosol respectively. P_r, P_a are the phase function for Rayleigh and aerosol respectively. r and k are the water-leaving radiance and the asymmetric factor respectively. μ_1 and are the cosine of satellite and the solar

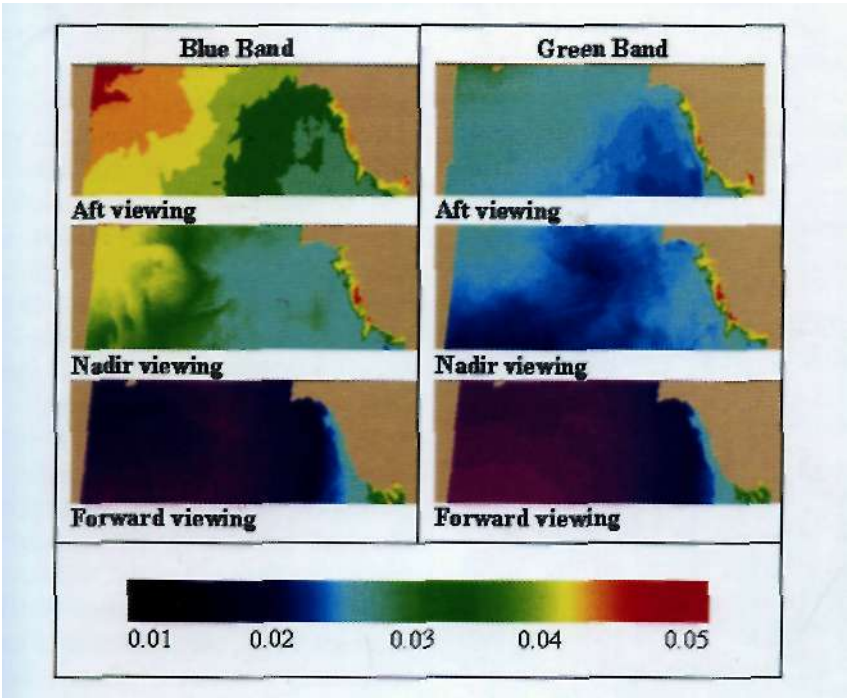

Figure 6. Surface Reflectance

zenith angle respectively. © is the scattering angle, k is assumed as $1 < k < 2$ for all possible calculations.

Due to spectral dependencies, To (A.) were extrapolated to respective bands (blue band and green band) of the MISR, while the surface reflectance is computed by Eq. (2) for three viewing directions (aft, nadir and forward) and shown in Fig. 6. For the all calculations, we make use of the MISR Level -3 AOT validated with the AIR-MISR data. The ranges of all these reflectances agree well with the 6S estimation shown in Fig. 5. For blue band, the aft viewing camera yields the reflectance values from 0.04 to 0.05, which are slightly larger than the ranges of 0.02 to 0.03 from the forward viewing camera. For these two directions, the resulting patterns are quite similar from the coastal regions to the open ocean. The nadir viewing result shows reflectance values from 0.03 to 0.04 and becomes identical with the aft viewing surface reflectance in the coastal regions. As compared with the forward and nadir results, the aft viewing reflectance exhibits somewhat larger uncertainty to the calibration error in the aft viewing camera (Bruegge, et al., 2004). However, the accuracy has not been, quantified yet. Estimation of AOT from the MISR archive contains some percentages of error which can be attributed to the surface reflectance which is avoided.

c. Chlorophyll-a estimation from MISR

The chlorophyll-a concentration is directly related to the surface reflectance ratio between different bands (Gordon, 1997). Though the MISR is not the ocean color sensor, its blue and green bands give information pertinent to the ocean color analysis. In a recent report on the MISR data archive (David, et al., 2001), attempts were also made to derive surface reflectance for the ocean application. We estimate the ocean surface reflectance using the single scattering approximation for three cameras (AF, AA and AN) and its accuracy is quantified. The concentration of chlorophyll-a (chl) is estimated using the following expression given below (Kahru and Mitchell, 1999)

$$chl = 10^{(a0+a1R+a2R^2+a3R^3+a4R^4)} + a_5 \quad \text{.....(3)}$$

where

$$R = \log_{10}(nL_w(\text{Blue}) / nL_w(\text{Green})) \quad \text{.....(4)}$$

In Eq. (3), aO through a5 are the regression coefficients. The above equation is the maximum band ratio and modified cubic polynomial equation. The regression coefficients are modified from O'Reilly et al 1998 (Kahru and Mitchell, 1999). The values are aO, a1, a2, a3, a4 and a5 are 0.565, -2.561, -1.051, -0.294, 5.561, -0.04 respectively. The unit of chlorophyll-a concentration is expressed in mg m-3. The resulting distributions from three viewing cameras are shown in Fig. 7. The same set of regression coefficients aO - a5 is used for deriving these concentration patterns.

In Figs.7 (a) - (c), similar distribution patterns are observed for three viewing directions, but the concentration values are different. The error may be slightly more or less in the case of the forward and aft cameras but the nadir camera estimates reflectance with a fair accuracy. High concentration of chlorophyll-a is observed in the coastal (case-2) waters due to intrusion of riverine water (the Indus river) and vertical stratification. Similar observations were reported in various literatures. Among the three viewing directions, nadir and aft results show identical pattern in the coastal regions, while the forward result exhibits various patterns in the open ocean. Although the chlorophyll concentration can be reasonably derived from the nadir observations in both coastal and open

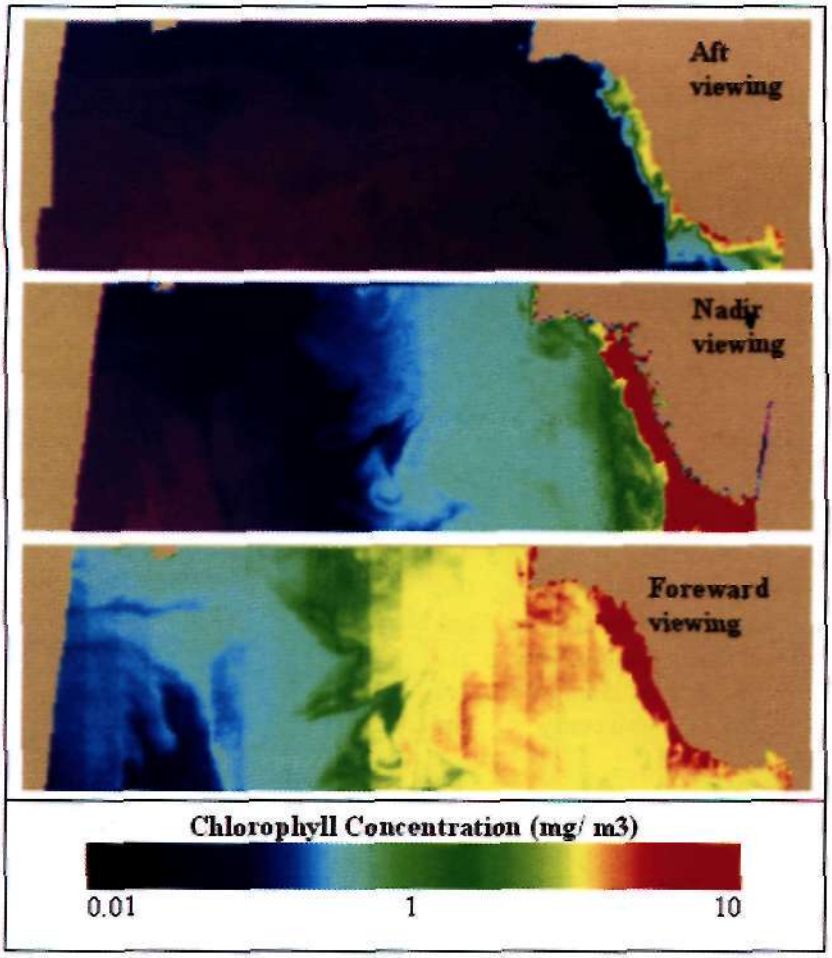

Figure 7 Chlorophyll-a concentration (mg/m^3)

ocean regions, there are small scale eddies in the open ocean revealed only from the forward observations. In the open ocean, the aft image shows the concentration assessment that is consistent with the nadir image. It is evident that while the nadir viewing camera reveals large scale eddies, small features such **as** meanders and small scale eddies are more clearly detected in the forward and aft viewing images. The accuracy of these chlorophyll-a concentrations can be estimated on the basis of the accuracies in the AOT retrieval from the MISR and the in-water algorithm.

Conclusions

The MISR sensor views the Earth using its different viewing direction cameras to observe the scattered sunlight. Not only it reveals the atmospheric constituents such as aerosols and clouds, but it also helps to estimate the reflectance properties of various targets. We can retrieve the AOT from the MISR data by the multi directional method. In this calculation we employ the 6S code to find both the AOT and surface reflectance by iterating the forward calculation. The obtained AOT, thus, agree with that provided by the NASA MISR archives. These AOT values were applied to all different viewing directions. The forward and aft

viewing results. Substituting the derived surface reflectance into the in-walcr algorithm, we obtain the ocean chlorophyll-a concentration. The pattern of the chlorophyll-a concentration shows good agreement with that of the surface reflectance derived from blue and green bands. Forward (aft) viewing observations overestimate (underestimate) the chlorophyll-a concentrations as compared with the nadir viewing results. This effect is conspicuous in case-1 waters.

Acknowledgement

The author would like to thank MISR group for providing data and deep appreciation to Prof. H. Kuze, for his constructive suggestion for making this manuscript. The author also like to thank Monbusho for funding scholarship to the author. This work is a collaborative work between chiba university and EORC/JAXA.

References

Brueggc, C J., W. A. Abdou, D. J. Diner, B. J. Gaitley, M. C. Helmlinger, R. A. Kahn, and J. V. Martonchik. 2004. Validating the MISR radiometric scale for the ocean aerosol science communities. In: Post-launch calibration of satellite sensors. S. A. Morain and A. M. Budge, (editors). A. A. Balkema Publishers, Leiden, Netherlands, pp. 103-115.

Chandrasekhar S- I960. Radiative Transfer. Dover Publications, New York.

Das, I., M. Mohan, K. Krishnamoorthy. 2002. Detection of marine aerosols with IRS-P4 Ocean Colour Monitor. Proc. Indian Acad. Sci (Earth. Planet. Sci.), lll(4):425-435.

David ct al. 2001. MISR Level 2 Aerosol Retrieval Algorithm Theoritical Basis. http://eospso.gsfc .nasa.gov/cos_homepage /for_scientists/atbd/docs/MISR/atbd.misr-09.pdf.

Gordon, H. R. and A. Y. Morel. 1983. Remote Assessment of Ocean Color for Interpretation of Satellite Visible Imagery: a Review. Springer-Vcrlag, New York).

Gordon, H. R.. 1997. Atmospheric correction of ocean color imagery in the Earth Observing System Era, Journal of Geophysical Research, 102(D14):17081-17106.

Gordon, H. R. and M. Wang. 1996. Retrieval of water leaving radiance and aerosol optical thickness over the oceans with SeaWiFS: a preliminary algorithm. Applied Optics, 33:443-452.

Gordon, H. R. and T. Zhang. 1996. How well can radiance reflected from the ocean-atmosphere system be predicted from measurements at the sea surface?. Applied Optics, 35:6527-6543.

Haltrin, V. I. 2002. One Parameter two term Heyney-Greenstein phase function for light scattering in seawatcr. Applied Optics, 41 (6): 1022-1028.

Kahru, M. and B. G- Mitchell. 1999. Empirical chlorophyll algorithm and preliminary SeaWiFS validation for California current. International Journal of Remote Sensing, 20(17):3423-3429.

Kaufman, Y. J., A. Gitelson, A. Kamieli, E. Ganor, R. S. Fraser, T. Nakajima, S. Martoo, and B. N. Holbcn. 1994. Size distribution and phase function of aerosol particles retrieved from sky brightness measurements. J. Geophys. Res., 99:10341-10356.

Lenobel, J. 1993. Atmospheric Radiative Transfer. A. Deepak Publishers, Hampton, VA. 532pp.

Nakajima, T.. M. Tanaka, and T. Yamauchi. 1983. Retrieval of optical properties of aerosols from aureole and extinction data. Applied Optics- 22:2951-2959.

Ramanathan, V. et al. 2000. Indian Ocean Experiment: An integrated analysis of the climate forcing and effects of the great Indo-Asian haze. J, Geophys. Res., 106(28):371-398.

Rasch. P. J., M. C. Barth, J. T. Kichl, S. E. Schwartz, and C. M. Bcnkovitz. 2000. A

description of the global sulfur cycle and its controlling processes in the National Center **for** Atmospheric Research Community Climate Model, Version 3. J. Geophys. Res., 105:1367-1385.

Vermote. E.. D. Tanre, J. L. Dcuzc, M. Herman, and J. J. Morcrcttc. 1997. Second Simulation of the satellite signal in the solar spectrum, 6S: An overview. IEEE Transactions on gcoscience and remote sensing, 35<3):675-686.

Wang, M. and H. R. Gordon. 1993. Retrieval of the columnar aerosol phase function and single scattering albedo from sky radiance over the ocean: simulations. Applied Optics, 32:4598-4609.